Monthly Notices
of the
ROYAL ASTRONOMICAL SOCIETY

MNRAS **466,** 2151–2160 (2017)
Advance Access publication 2016 December 13

doi:10.1093/mnras/stw3245

History of the mass ejection in K4-37: from the AGB to the evolved planetary nebula phase

L. F. Miranda,[1⋆] P. F. Guillén,[2] L. Olguín[3] and R. Vázquez[2]

[1] *Instituto de Astrofísica de Andalucía – CSIC, C/ Glorieta de la Astronomía s/n, E-18008 Granada, Spain*
[2] *Instituto de Astronomía, Universidad Nacional Autónoma de México, Apdo. Postal 877, 22800 Ensenada, B.C., Mexico*
[3] *Departamento de Investigación en Física, Universidad de Sonora, Blvd. Rosales Esq. L.D. Colosio, Edif. 3H, 83190 Hermosillo, Son., Mexico*

Accepted 2016 December 9. Received 2016 December 9; in original form 2016 October 24

ABSTRACT

We present narrow-band, broad-band and *Wide-field Infrared Survey Explorer* (*WISE*) archive images, and high- and intermediate-resolution long-slit spectra of K4-37, a planetary nebula that has never been analysed in detail. Although K4-37 appears bipolar, the morphokinematical analysis discloses the existence of three distinct axes and additional particular directions in the object, indicating that K4-37 is a multi-axis planetary nebula that has probably been shaped by several bipolar outflows at different directions. A 4–6 $M_{\odot}$ main-sequence progenitor is estimated from the derived high nebular He and N abundances, and very high N/O abundance ratio (∼2.32). The general properties are compatible with K4-37 being a highly evolved planetary nebula located at ∼14 kpc. The *WISE* image at 22 μm reveals K4-37 to be surrounded by a large (∼13 × 8 pc^2) elliptical detached shell probably related to material ejected from the asymptotic giant branch (AGB) progenitor. The observed elliptical morphology suggests deformation of an originally spherical AGB shell by the interstellar medium magnetic field or by the influence of a companion. We compare K4-37 and NGC 6309 and found remarkable similarities in their physical structure but noticeably different chemical abundances that indicate very different progenitor mass. This strongly suggests that, irrespective of the initial mass, their (presumably binary) central stars have shared a very similar mass ejection history.

Key words: circumstellar matter – ISM: jets and outflows – planetary nebulae: individual: K4-37.

1 INTRODUCTION

It is well known that planetary nebulae (PNe) originate from asymptotic giant branch (AGB) and post-AGB stars with low- and intermediate-mass ($\lesssim$8–10 $M_{\odot}$) main-sequence progenitors once the central star becomes hot enough to photoionize the envelope ejected during the AGB phase. It is also well known that this process, when applied to single star evolution, can hardly explain the dramatic transformation of a spherical AGB envelope into the varied and complex morphologies observed in a noticeable number of PNe (e.g. Balick & Frank 2002).

During the last four decades, the formation of PNe has been understood within the interacting stellar wind model (ISW; Kwok, Purton & Fitzgerald 1978; Balick 1987). This model has probed its ability to explain many of the features observed in PNe (Balick & Frank 2002, and references therein). However, multiple, highly collimated and axisymmetric structures in PNe have always presented difficulties to be explained within the ISW scenario. Nowadays, in addition to wind–wind interaction, it is recognized that the formation of complex PNe requires the action of collimated outflows that distort an originally spherical AGB envelope (Sahai & Trauger 1998). In this context, binary central stars were always thought to be determining the formation of complex PNe (e.g. Morris 1981; Soker & Livio 1994). The importance of binary central stars in PN formation is receiving strong support with the detection of new post-common envelope binary central stars associated with complex PNe (Miszalski et al. 2009; Miszalski 2012; Jones 2016; and references therein). Evolution in a common envelope provides many of the basic ingredients thought to be involved in the formation of complex PNe, as accretion discs, highly collimated outflows and magnetic fields (García-Segura et al. 1999; Dennis et al. 2008; de Marco 2009; and references therein).

Nowadays, about 3500 PNe are known in the Galaxy (Parker, Bojičić & Frew 2016). However, many of them still lack an analysis that allows us to place them within the evolutionary sequence and to carry out comparisons with other PNe, which could provide information to disentangle the possible key processes involved in the formation of the different kinds of PNe. Given the enormous variety of properties (e.g. morphology, kinematics, chemical abundances, physical conditions) exhibited by PNe, increasing the number of well-analysed objects may contribute to shed light on the processes involved in the AGB to PN transition.

⋆ E-mail: lfm@iaa.es

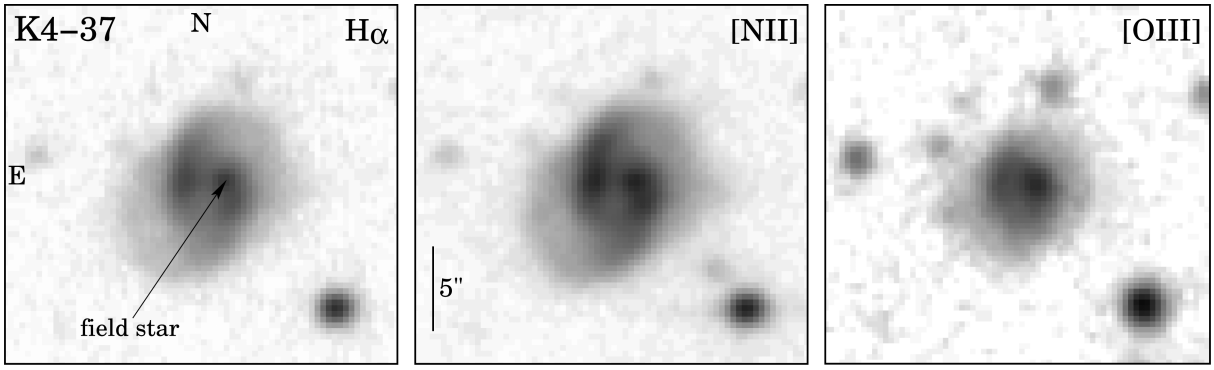

Figure 1. Grey-scale reproductions of the 1998 Hα and [N II], and 2016 [O III] images of K4-37. The grey levels are logarithmic. North is up, east to the left. A field star is arrowed in the 1998 Hα image, which has been identified as a star (and not as a nebular knot) thanks to the intermediate-resolution, long-slit spectrum (Section 2.3). The size of the field shown in the three panels is 23 × 21.5 arcsec^2.

K4-37 (PN G066.9+02.2; α(2000.0) = 19^{h}51^{m}00^s.6; δ(2000.0) = +31°02′29″) is a PN that has never been analysed in detail. It was discovered by Kohoutek (1965) and its PN nature can be guessed from the emission line fluxes listed in the Strasbourg ESO Catalogue (Acker et al. 1992). According to this catalogue, the nebula presents very strong [N II] and [S II], moderate [O III] and absent He II λ4686 emission lines, indicating a very low-excitation PN. Except for these data, information about the characteristics and properties of K4-37 is lacking in the published literature. The object was imaged by us many years ago in our programmes to study compact PNe (e.g. Miranda et al. 1997, 2000, 2001; Vázquez et al. 2002) and it showed a simple and less interesting bipolar morphology. However, the acquisition and analysis of new data, and inspection of the *Wide-field Infrared Survey Explorer* (*WISE*) archive (Wright et al. 2010) have revealed noticeable properties in this PN. In this paper, we present the data, analysis and results that we have obtained for K4-37.

2 OBSERVATIONS AND RESULTS

2.1 Optical imaging

Narrow-band images of K4-37 were obtained during 1998 July 7–9 with Calar Alto Faint Object Spectrograph (CAFOS) at the Calar Alto Observatory. The detector was LORAL 2k × 2k CCD with a plate scale of 0.33 arcsec pixel^{-1}. Three filters were used: Hα (FWHM = 15 Å), [N II] (FWHM = 19 Å) and [O III] (FWHM = 25 Å). Exposure time was 600 s for each filter. The spatial resolution, determined by the full width at half-maximum (FWHM) of field stars, is 1.2 arcsec in the Hα and [N II] images and 3 arcsec in the [O III] one.

Additional narrow-band images were obtained also with CAFOS in 2014 June 4 using an Hα+[N II] filter (FWHM = 50 Å) and an exposure time of 3 × 600 s, and in 2016 May 3 using an [O III] filter (FWHM = 25 Å) and an exposure time of 2 × 900 s. In 2014 and 2016, the detector was a SITe 2k × 2k CCD with a plate scale of 0.53 arcsec pixel^{-1}. The FWHM of the field stars in the Hα+[N II] image is 0.9 arcsec, lower than twice the pixel size, suggesting that the true spatial resolution of this image is better than 0.9 arcsec. In the 2016 [O III] image, the spatial resolution is 1.4 arcsec.

The images were cosmic ray cleaned, bias subtracted and flat fielded using standard routines within the MIDAS package. To gain a better view of the morphology of K4-37, we have used the Richardson–Lucy algorithm in the MIDAS package, to deconvolve the Hα+[N II] image. A well-exposed field star in the image was used as point spread function, and iteration was stopped when artefacts appeared in the deconvolved image. After 30 iterations, we obtained a deconvolved Hα+[N II] image with a spatial resolution of ∼0.5 arcsec.

The 1998 Hα and [N II] images together with the 2016 [O III] image are shown in Fig. 1. The original and deconvolved Hα+[N II] images are presented in Fig. 2. The nebula shows a bipolar shape with a size of ∼12 × 6.5 arcsec^2 in Hα and [N II], somewhat smaller in [O III], and the major axis oriented at position angle (PA) ∼ −40°. Nevertheless, faint emission can be detected in an ∼18 × 11 arcsec^2 area. The images show a point-symmetric intensity distribution in the bipolar lobes approximately along the north–south direction. A torus traces the equatorial plane of the nebula, which contains two bright knots located symmetrically with respect to the centre of the object and oriented at PA ∼ 60°. Due to the point-symmetric regions of the lobes, the axis of the torus seems to be oriented close to the east–west direction. However, the deconvolved Hα+[N II] image does show that its axis is oriented similar to that of the bipolar lobes. The size of the torus is ∼4 × 2 arcsec^2 and some distortions can be recognized towards its southeastern side.

More details about the morphology of K4-37 can be recognized in the original and deconvolved Hα+[N II] images (Fig. 2). These images show a noticeably limb-brightening and a knotty structure in the bipolar lobes. Moreover, the northwestern lobe is clearly distorted or broken towards the west where an elongated feature is observed up to ∼7.3 arcsec from the centre, which clearly deviates from the lobe geometry. An eastern counterpart cannot be recognized in the southeastern lobe (Fig. 2), but we note that the region along PA ∼ 90° protrudes and does not follow the lobe geometry. In fact, the southeastern lobe can be traced up to ∼5.7 arcsec from the centre along PA ∼ 90° whereas it extends only ∼4 arcsec at PA ∼ 180°. The distorted regions subtend an angle of ∼30° as seen from the centre. From the images in Fig. 2, two different axes are identified in K4-37: one along PA ∼ −40°, defined by the main axis of the lobes and bright torus, and another one along PA ∼ 270° (or ∼90°), defined by the distortions of the bipolar lobes. Besides, the point-symmetric features suggest additional particular directions in the nebula.

The central star of K4-37 has never been identified and is neither observed in our narrow-band images. Central stars with V or B magnitudes $\lesssim 17^m$ can be detected in (narrow-band) Hα or [O III] images with moderate exposure times, which implies that the central star of

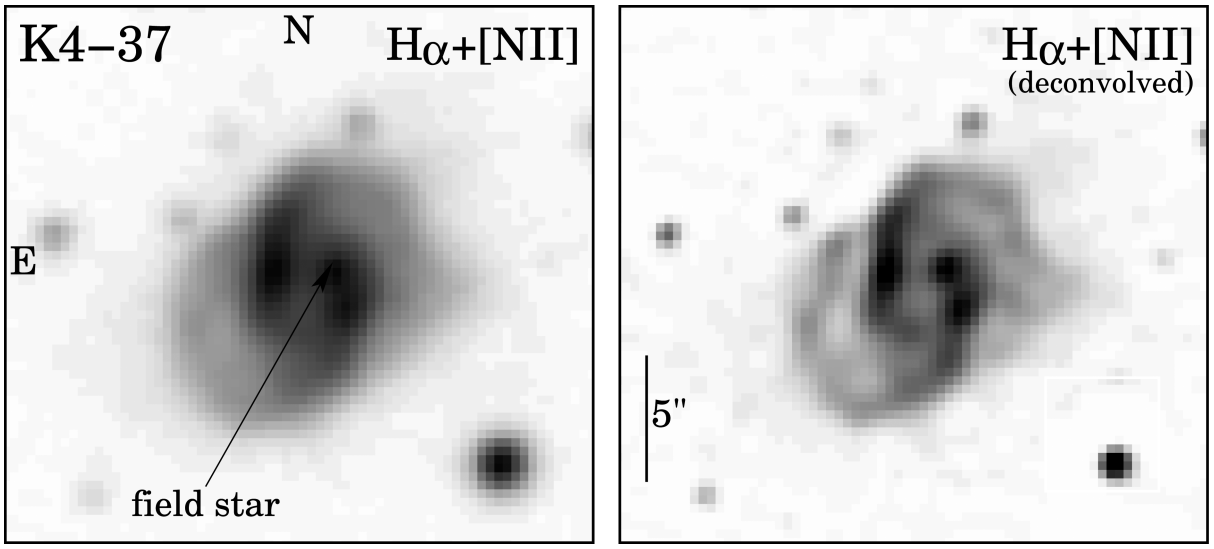

Figure 2. Grey-scale reproductions of the 2014 original (left) and deconvolved (right) Hα+[N II] image of K4-37. The grey levels are logarithmic. North is up, east to the left. A field star is arrowed in the Hα+[N II] original image (see caption of Fig. 1). The size of the field shown in the two panels is 23 × 21.5 arcsec^2.

K4-37 should be very faint. In an attempt to detect it, we obtained an image of K4-37 with CAFOS in 2016 May 3 using a Johnson *B* filter and an exposure time of 1200 s, under seeing conditions of ∼1.5 arcsec. No star can be recognized in our *B* image close to the centre of the object, where the central star could be expected, which would imply a lower limit of ∼20^m for its *B* magnitude. On the other hand, it is well known that central stars may be displaced from the nebular centre (e.g. Soker 1994; Tweedy & Napiwotzki 1994; Soker, Rappaport & Harpaz 1998; Chiotellis et al. 2016). We note that the images of K4-37 show a star at ∼1.7 arcsec from nebular centre (Figs 1 and 2). Its spectrum indicates a K-type star (see Section 2.3). A (somewhat speculative) alternative to the non-detection of a star at the nebular centre could be that the central star and the K-type star constitute a (non-resolved) binary system that has moved since the nebula was formed. If this was the case, the angular distance to the centre and the age of the nebula (∼10^4 yr, Section 3.2) would imply a proper motion of ∼0.17 mas yr^{-1} for the pair, corresponding to a tangential velocity of ∼11 km s^{-1} (at a distance of 14 kpc, see Section 3.2). If so, the large distortion of the nebula towards the west, as compared with that towards the east, could be partially due to that motion. In any case, further efforts to detect the central star of K4-37 would be very valuable.

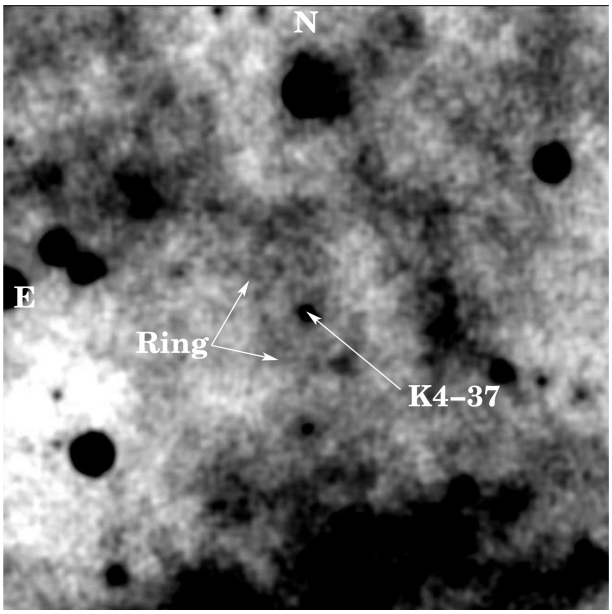

Figure 3. Grey-scale reproduction of the *WISE* image at 22 μm (*W*4) around K4-37 (arrowed). Grey levels are linear. North is up, east to the left and the field of view is 15 × 15 arcmin^2. The elliptical ring-like structure is arrowed.

2.2 *WISE* imaging

To complement our analysis, we have retrieved the images of K4-37 obtained with the *WISE* satellite in the four bands: *W*1 (3.4 μm), *W*2 (4.6 μm), *W*3 (12 μm) and *W*4 (22 μm), in a field of 15 × 15 arcmin^2 centred on the object.

K4-37 itself is not resolved in the *WISE* images owing their relatively low spatial resolution (6.1–12 arcsec) and the small size of the object. In addition, the field star observed in the optical images (Fig. 2) is bright at 3.4–22 μm and this star and the nebula are indistinguishable in the *WISE* images. The more interesting result is observed in the *W*4, band a reproduction of which is shown in Fig. 3 . K4-37 appears embedded in a complex nebular environment in which stands out an elliptical ring-like structure surrounding the optical PN. Emission from the ring-like structure is also observed in the *W*3 band but more diffuse and fainter than in the *W*4 one, and is not observed in the *W*1 and *W*2 bands (not shown here). The elliptical ring-like structure (hereafter referred to as the 22 μm ring) is open (or very faint) towards the north-west, contains a bright spot towards the south-west, and presents a complex region towards the north-east where it seems to contact an ambient filament. The edge of the 22 μm ring is relatively bright but the emission is also detected inside it. The complex northern region makes it difficult to obtain accurately the orientation and major axis of this structure. Nevertheless, its minor axis appears oriented close to PA ∼ −60° and is ∼2 arcmin in size, its major axis is ∼2.9–3.6 arcmin in size as measured at PA 30° (in the following we will adopt a major axis of 3.2 arcmin), while a size of ∼2.4 arcmin is measured at PAs 75° and 165°. From the image in Fig. 3, an association, and not a

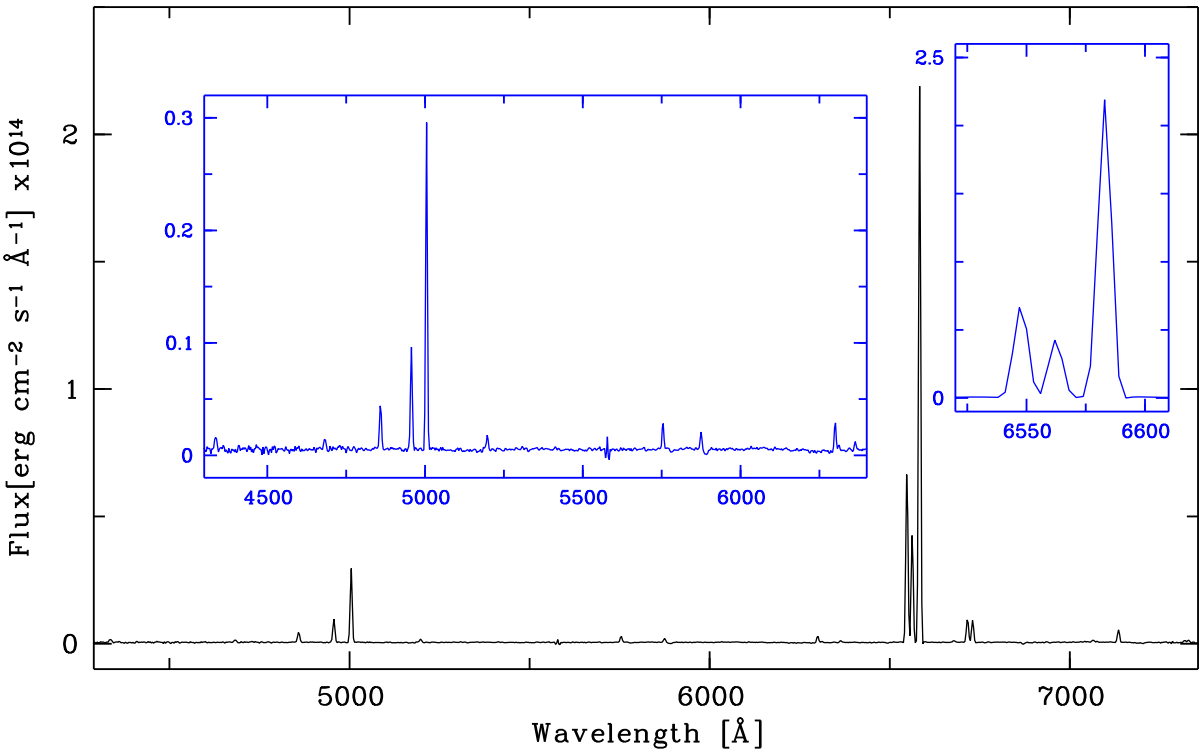

Figure 4. Flux-calibrated spectrum of K4-37. The left inset shows the spectrum between 4300 and 6400 Å and the right inset is the [N II] λλ6548, 6583 and Hα region.

superposition chance, between the 22 μm ring and the optical nebula is strongly suggested because the 22 μm ring, the only closed structure observed in the field, is well centred on K4-37. Nevertheless, the optical nebula seems to be slightly displaced towards the south-east with respect to the possible centre of the 22 μm ring, which is difficult to define because of its complex northern region. The large difference in sizes between the optical nebula and the 22 μm ring strongly suggests that the latter should correspond to a much older ejection than that involved in the formation of the main nebula. As we will discuss below (Section 3.3), the 22 μm ring probably represents mass ejected from the AGB progenitor of K4-37. We note that the detection of this structure at 22 μm suggests dust as origin of its emission.

2.3 Intermediate-resolution long-slit spectroscopy

Intermediate-resolution, long slit-spectra of K4-37 were obtained on 2008 June 8 with the Boller & Chivens spectrograph mounted on the 2.1 m telescope at the San Pedro Martir Observatory (OAN-SPM),[1] using the SITe3 CCD (plate scale 24 μm pix^{-1}), with a 1k × 1k pixel array as a detector. We used a 400 lines mm^{-1} dispersion grating along with a 2.5 arcsec slit width, giving a spectral resolution (FWHM) of ∼6.5 Å and covering the 4300–7400 Å spectral range. The slit was centred on the nebula and oriented at PA 90°. Four spectra were obtained with an exposure time of 1800 s each. Spectra reduction was carried out following standard procedures in XVISTA.[2] In particular, the median of the four spectra was first derived and then it was subtracted from each individual spectrum to detect and eliminate cosmic rays manually. Finally, the cleaned spectra were added to get a final spectrum with a total exposure time of 7200 s. Spectrophotometric standard stars were observed in the same night for flux calibration purposes. Seeing was ∼2.5 arcsec during the observations.

The field star overimposed on the nebula (Figs 1 and 2) is covered by the slit. The spectrum indicates a K-type for this star. We have fitted the continuum of this star and subtracted it from the integrated nebular spectrum. The contribution of the stellar absorption lines to the Balmer nebular emission lines is difficult to evaluate because a more precise spectral type cannot be deduced for the field star. Nevertheless, from other observed absorption lines in the stellar spectrum, we estimate that this contribution should be lower than ∼2 per cent and, therefore, it is not critical in the analysis of the nebular emission spectrum.

Fig. 4 shows the integrated spectrum of K4-37 and Table 1 lists the emission line intensities, their errors and several parameters, as determined with the program ANNEB, a description of which can be found in Olguín et al. (2011). Briefly, we used the extinction law of Seaton (1979) and assume case B recombination to start an iterative process until the values of the logarithmic extinction coefficient $c(\mathrm{H}\beta)$, electron temperatures T_e[N II] and T_e[O III] obtained from the [N II] and [O III] emission line ratios, respectively, and electron

[1] The Observatorio Astronómico Nacional at the Sierra de San Pedro Mártir (OAN-SPM) is operated by the Instituto de Astronomía of the Universidad Nacional Autónoma de México.

[2] XVISTA was originally developed as Lick Observatory Vista. It is currently maintained by Jon Holtzman at New Mexico State University and is available at http://ganymede.nmsu.edu/holtz/xvista.

Table 1. Dereddened emission line intensities in K4-37 in units of $I_{H\beta} = 100.0$.

Ion	λ	$f(\lambda)$	$I(\lambda)$
H γ	4340	0.129	64.5 ± 5.9
[O III]	4363	0.124	12.2 ± 3.7
He II	4686	0.042	29.9 ± 2.8
Hβ	4861	0.000	100.0 ± 2.3
[O III]	4959	–0.024	194.5 ± 3.4
[O III]	5007	–0.035	572.5 ± 9.5
[N I]	5199	–0.075	26.0 ± 1.1
[N II]	5755	–0.192	24.0 ± 0.7
He I	5876	–0.216	15.3 ± 0.6
[O I]	6300	–0.285	20.2 ± 0.6
[S III]	6312	–0.287	5.5 ± 0.4
[O I]	6363	–0.294	5.5 ± 0.3
[N II]	6548	–0.321	465.9 ± 13.0
Hα	6563	–0.323	283.9 ± 8.0
[N II]	6583	–0.326	1414.8 ± 39.8
He I	6678	–0.339	5.2 ± 0.3
[S II]	6716	–0.343	60.0 ± 1.8
[S II]	6731	–0.345	53.6 ± 1.6
He I	7065	–0.383	4.8 ± 0.3
[Ar III]	7136	–0.391	25.7 ± 0.9
[O II]	7320	–0.411	4.9 ± 0.3
[O II]	7330	–0.412	5.1 ± 0.3
log F(Hβ) (erg cm^{-2} s^1)			−16.23 ± 0.03
c(Hβ)			1.71 ± 0.03
T_e[N II] (K)			11000 ± 300
T_e[O III] (K)			15800 ± 2450
N_e[S II] (cm^{-3})			370 ± 120

density, N_e[S II] obtained from the [S II] λλ6716, 6731 emission lines, converge to their final values that are listed in Table 1.

Fig. 4 and Table 1 show the extreme low-excitation of K4-37 with [N II]/Hα and [S II]/Hα line intensity ratios of ∼6.6 and ∼0.4, respectively, and prominent [N I] and [O I] emission lines as compared with that usually observed in PNe (see Section 3.1). The [O III]/Hβ line intensity ratio presents a moderate value of ∼7.7. Noticeably, the He II λ4686 emission line is also detected in our spectrum and indeed with a relatively strong intensity of about a third of Hβ, suggesting a relatively hot central star. Finally, the electron temperatures are quite typical of PNe, while the electron density is very low (see Table 1), indicating a very evolved PNe.

Ionic and elemental abundances were derived using the values of N_e[S II] and T_e[N II] in Table 1, and are listed in Table 2. The ICF method of Kingsburgh & Barlow (1994) has been used as implemented in ANNEB. The high He (He/H ∼0.145) and N (N/H ∼6.3 × 10^{-4}) abundances make K4-37 a typical type I PN (Peimbert 1990). Sulphur and argon abundances are in the range of the values observed in PN and type I PNe (e.g. Kingsburgh & Barlow 1994). What makes K4-37 particularly interesting is the high value of the N/O abundance ratio of ∼2.32 that is among the highest ones observed in PNe (see e.g. Pottasch, Beintema & Feibelman 2000; Akras et al. 2016 and references therein) and indicates an extreme nitrogen enrichment. The high He and N abundances and N/O abundance ratio imply an intermediate mass progenitor. We have compared the values in Table 2 with the models for stellar yields by Karakas (2010) to estimate an initial mass of 4–6 M$_\odot$ for the main-sequence progenitor of K4-37.

Table 2. Ionic and elemental abundances by number in K4-37.

Ion	Abundance
He$^+$ (×10^2)	12.060 ± 0.397
He^{2+} (×10^2)	2.42 ± 0.22
O^0 (×10^4)	0.26 ± 0.01
O$^+$ (×10^4)	0.93 ± 0.04
O^{2+} (×10^4)	1.48 ± 0.02
N^0 (×10^5)	2.61 ± 0.11
N$^+$ (×10^4)	2.15 ± 0.04
S$^+$ (×10^6)	2.21 ± 0.05
S^{2+} (×10^6)	8.93 ± 0.64
Ar^{2+} (×10^6)	1.90 ± 0.06
Element	**Abundance**
He/H	0.145 ± 0.005
O/H (×10^4)	2.72 ± 0.06
N/H (×10^4)	6.31 ± 0.36
Ar/H (×10^6)	3.55 ± 0.79
S/H (×10^5)	1.25 ± 0.07

2.4 High-resolution long-slit spectroscopy

High-dispersion optical spectra were obtained with the Manchester Echelle Spectrometer (Meaburn et al. 2003) and the 2.1 m (f/7.5) telescope at the OAN-SPM Observatory during 2004 July 29–30. A SITe CCD with 1k×1k pixels was used as detector. The slit length was 6.5 arcmin and its width was set to 150 μm (2 arcsec). A 2×2 binning was used, leading to a spatial scale of 0.66 arcsec pixel^{-1} and a spectral scale of 0.1 Å pixel^{-1}. This spectrograph has no cross-dispersion, consequently, a $\Delta\lambda = 90$ Å bandwidth filter was used to isolate the 87th order covering the spectral range that includes the Hα and [N II] λλ6548, 6583 emission lines. Spectra were obtained with the slit centred across the centre of the nebula and oriented at PAs −40° and +90°. Exposure time for each spectrum was 1200 s. The spectra were wavelength calibrated with a Th–Ar arc lamp to an accuracy of ±1 km s^{-1}. The FWHM of the arc lamp emission lines was measured to be ≃ 12 km s^{-1} that corresponds to the achieved spectral resolution. Seeing was ∼2 arcsec during the observations. Reduction of the spectra was carried out with standard routines in the IRAF package.

Fig. 5 presents position–velocity (PV) maps of the [N II] λ6583 emission line at the two observed PAs. From these high-resolution spectra, the systemic velocity of K4-37 was measured by co-adding 2.4 arcsec around the central position of the emission line features observed at each PA, and finding the central radial velocity of the resulting line profile. The estimates for the systemic velocity in both spectra and from the Hα and [N II] λλ6548, 6583 emission lines are consistent with each other after heliocentric and LSR corrections, and its mean value is $V_{HEL} = -23.7 \pm 1.5$ km s^{-1} ($V_{LSR} = -5.3 \pm 1.5$ km s^{-1}).

The [N II] emission feature in the PV maps (Fig. 5) is dominated by two intensity maxima that correspond to the equatorial ring. The PV map at PA −40° shows two velocity components at each spatial position, as expected from a bipolar shell. The velocity splitting is small and varies between ∼22 and ∼30 km s^{-1}. At PA 90°, velocity splitting is clearly observed around the centre of the line feature but is difficult to recognize at larger angular distances. The long-slit spectrum at PA 90° covers the distorted region towards the west (Fig. 2). In fact, the [N II] emission feature in the PV map at PA 90° is much more extended towards the west than towards the east, in consonance with the images (Fig. 2). If the western nebular regions

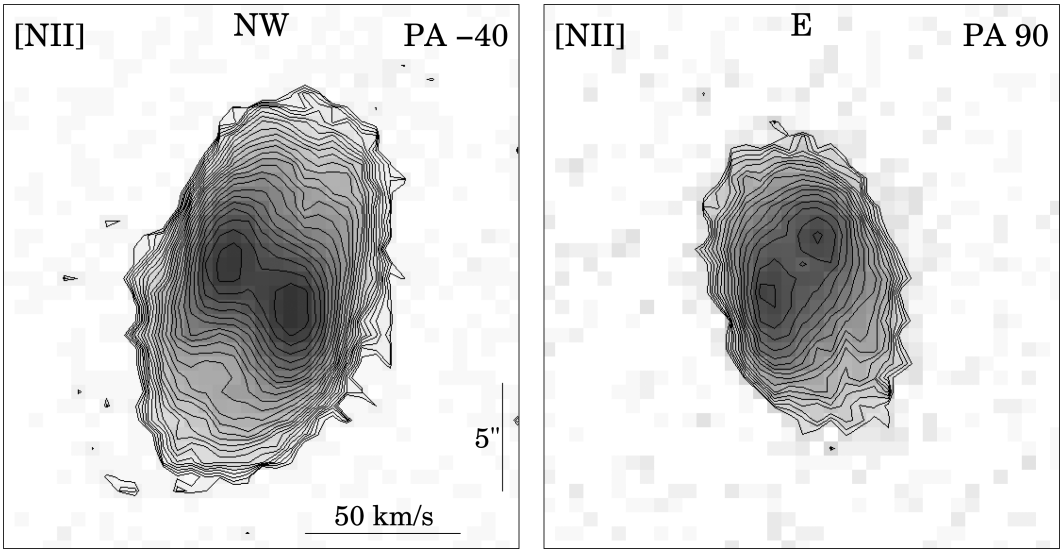

Figure 5. Grey-scale and contours PV maps of the [N II] λ6583 emission line at the two observed PAs (upper right). The grey levels and contours are logarithmic. Spatial and velocity scales are identical in both panels and indicated in the left one.

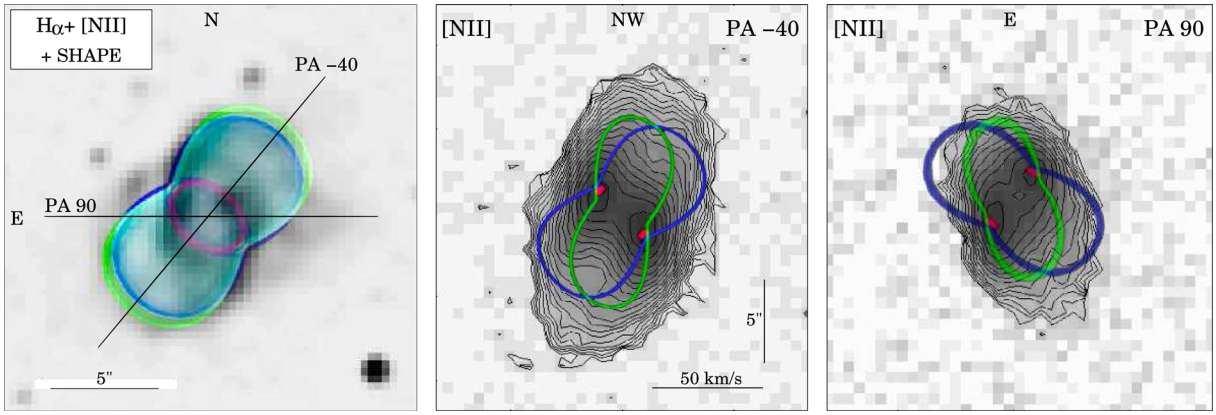

Figure 6. Grey-scale Hα+[N II] deconvolved image (left) and grey-scale and contours PV maps of the [N II] λ6584 emission line (middle and right). The grey levels and contours are logarithmic. The orientation of the long slits are plotted on the image (slit width not to scale), and the PV maps contain information about the orientation, and spatial and velocity scales, the latter two being identical in the middle and right-hand panels. Overimposed on the panels are the results of SHAPE: red colour corresponds to the equatorial torus, blue colour to the bipolar lobes assuming homologous expansion velocity and green colour to the bipolar lobes assuming non-homologous expansion velocity and an inclination angle for the bipolar lobes different from that of the torus (see text for details).

have been distorted, as the images show, its kinematics may have been distorted, too, which may explain the lack of velocity splitting, as expected from a bipolar shell.

To extract more information from the PV maps, we used the tool SHAPE (Steffen et al. 2011) to find the morphokinematic parameters that are able to reproduce simultaneously the observed morphology and PV maps. It should be emphasized that we did not try to reproduce with SHAPE all the observed features in the PV maps and image in detail as, e.g. changes of intensity (point-symmetric regions, bright knots), spatial and velocity widths of the features and distortions of the structures. Rather, we try to reproduce the variation of the radial velocity (two components) as a function of the spatial position, as observed in the PV maps, and the basic shape (projected contour) of the bipolar lobes and torus, as observed in the image. In Fig. 6, we show the deconvolved Hα+[N II] image and [N II] PV maps of K4-37 together with the results of SHAPE assuming a thin bipolar shell with a homologous expansion velocity law, i.e. expansion velocity ($V_{\rm exp}$) proportional to the radius (r) at each point of the nebula [$V_{\rm exp}(r) = K \times r$] and narrow slits (1 arcsec) at PAs –40° and 90° (but see below).

The equatorial torus is quite well reproduced with a circular structure of 1.9 arcsec in radius, expansion velocity of 15.3 km s^{-1}, and a tilt for its axis of 45° with respect to the plane of the sky (red colour in Fig. 6). These parameters imply $K \sim$8.0 km s^{-1} arcsec^{-1}. When we applied this law to the bipolar lobes, we found that their kinematics cannot be reproduced satisfactorily, even though their morphology can be reproduced acceptably (blue colour in Fig. 6). It is clear that the kinematics of the bipolar lobes predicted assuming homologous expansion results to be very different from the observed one. First, we have considered whether a slit width of 2 arcsec (as we used for the long-slit spectra, see above) could have an effect on the resulting shape of the blue lines in Fig. 6. However, the use of a 2 arcsec slit produces virtually the same results as shown in Fig. 6, except that the blue lines become slightly thicker inwards as a result of including nebular regions at both sides of the main axis, which have somewhat lower radial velocities than along the

main axis. Other effects, as, e.g. smoothing due to seeing, may also increase the thickness of the blue lines but the *apparent tilt* of these lines in the PV maps *remains unchanged*. Then, we have modified (one by one and simultaneously) several parameters involved in the analysis (e.g. size of the polar axis, polar expansion velocity, inclination angle of the polar axis, in all cases also with a 2 arcsec slit width) and our conclusion is that reproducing the morphokinematics of the bipolar lobes requires that the main axis of the lobes is not perpendicular to the plane of the torus, and, in addition, that a non-homologous expansion law should be considered. In Fig. 6 (green colour), we also show the morphology and kinematics expected if the main axis of the lobes is tilted by 20° with respect to the plane of the sky, the semimajor axis is 5.3 arcsec, and the polar expansion velocity is 34 km s^{-1}. These parameters provide a much more acceptable reproduction of the kinematics observed in the PV maps and keep an acceptable representation of the morphology of the lobes as well. They also imply K ∼6.4 km s^{-1} arcsec^{-1} for the bipolar lobes, which is sensibly different from that obtained for the equatorial torus. We note that the western region of the PV map at PA +90° is difficult to reproduce (Fig. 6), and emission is observed at higher redshifted radial velocities than the predicted ones. This suggests that the distorted region could be more tilted than the axis of the lobes (i.e. >20° with respect to the plane of the sky), but a more precise determination would require spectra at higher spectral and spatial resolution. We have also checked the range of tilt angles capable to provide a reasonable reproduction of the observed morphokinematics and found that the deduced tilt angles are correct within ∼ ± 3° for the axis of the bipolar lobes and ∼ ± 1°.5 for the axis of the torus. These uncertainties are much smaller than the difference in tilt angles (∼25°), supporting that the difference is real. Finally, we note that the expansion velocities obtained in K4-37 (∼15–35 km s^{-1}), are noticeable lower than those observed in other bipolar PNe.

The morphokinematical analysis has disclosed the presence of two different axes where only one is observed in the images as the main bipolar axis. By chance, due to our line of sight, the axes of the torus and bipolar lobes appear aligned on the plane of the sky at about the same PA (∼–40°), but they present different tilts with respect to the observer (see also Section 3.4 for the case of NGC 6309). These two axes add to the axes of the distortions of the bipolar lobes and the orientation of the point-symmetric regions, which are all different from each other. According to these results, K4-37 may be better classified as a multi-axis PN rather than among bipolar PNe with a single axis.

The non-homologous expansion found in K4-37 is worth mentioning. The idea that PNe expand in a homologous manner has prevailed for long time mainly due to the fact that a simple homologous expansion velocity law is able to reproduce the observed PV maps of many PNe in a quite satisfactory manner. Nevertheless, PNe are known in which such a law is unable to reproduce the observed PV maps (e.g. Miranda et al. 1999; Steffen, García-Segura & Koning 2009; Steffen et al. 2013; Bermúdez 2015). In these cases, the action of collimated outflows on the shell and interaction between the stellar wind and an inhomogeneous shell have been invoked to explain the non-homologous expansion (see references above). In this context, the formation of the bipolar lobes of K4-37 seems to require a focused wind/outflow along a direction that is not perpendicular to the equatorial bright torus. In PNe, these kind of outflows are usually related to binary central stars. The possibility that at least in some PNe, non-homologous expansion could be suggesting a binary central star should be investigated.

From the morphokinematic parameters, we obtain kinematical ages of ∼590×D[kpc] yr and ∼740×D[kpc] yr for the torus and bipolar lobes, respectively, that seem to imply that the formation of the bipolar lobes has preceded that of the torus. However, given the uncertainties involved in the analysis, we will consider a mean value of 665×D[kpc] yr for the kinematical age of K4-37. As of the 22 μm ring, if we assume a constant expansion velocity of 15 km s^{-1} (typical of AGB envelopes), its kinematical age is ∼3.1×10^4×D[kpc] yr, much larger than that of the bipolar nebula.

3 DISCUSSION

3.1 The evolutionary status of K4-37

If the global properties derived in the previous sections are considered, K4-37 seems to find its right place among the group of highly evolved PNe recently analysed by Akras et al. (2016, hereafter AK16). Tables 3 and 4 in AK16 and Tables 1 and 2 in this work show the common properties. These PNe, including K4-37, show very strong [N II] and [S II] emissions that place them in the lower-left region of the diagram log(Hα+[N II]) versus log(Hα+[S II]) (see fig. 9 in AK16). AK16 call the attention to the presence of unusually strong [N I], [O I] emission lines in their sample of highly evolved PNe, which suggest a contribution of shock excitation (see also Akras & Gonçalves 2016). K4-37 presents [N I] and [O I] to Hβ line intensity ratios comparable to those in the sample by AK16, and, therefore, shocks are probably contributing to the line emission. These PNe also present high He and N abundances, and high N/O abundance ratios, indicating progenitors of ∼5 M$_\odot$, and very low electron densities (AK16; see Section 2.3). To these common characteristics, we add the presence of a relatively strong He IIλ4686 nebular emission (He IIλ4686/Hβ ∼0.2–0.5; Table 1; AK16 and references therein). This is probably related to the high effective temperature of their central stars (AK16). Although the central star of K4-37 has not been detected, its presumable faintness and relatively strong He IIλ4686 nebular emission suggest that it could be of low luminosity and high effective temperature, as those in the sample analysed by AK16.

3.2 The distance of K4-37

We have obtained a kinematical age of 665×D[kpc] yr for K4-37 that depends on its distance (Section 2.4). Although the distance is unknown, the resulting kinematical age should be compatible with K4-37 being a highly evolved PN. If, as a first approximation, we assume a kinematical age of >10000 yr as representative of a highly evolved PN (see AK16), the distance to K4-37 is >15 kpc. A more confident distance can be obtained by using the recent surface brightness–radius relationship by Frew, Parker & Bojičić (2016), the observed Hα flux and c(Hβ) (Table 2), and a mean nebular radius of ∼6 arcsec. With these values, the distance is ∼14 kpc and, consequently, the kinematical age is ∼9300 yr, compatible with a highly evolved PN.

For 14 kpc, the size of the nebula is ∼0.72×0.26 pc^2, very much smaller than the size of the 22 μm ring that amounts ∼13×8 pc^2 and whose kinematical age is of ∼4.3×10^5 yr. Taking into account the age of the nebula and that a 4–6 M$_\odot$ star traverses the post-AGB phase in $\lesssim$100 yr (Blöcker 1995), the kinematical age of the 22 μm ring places its formation in the AGB phase of the progenitor of K4-37.

Finally, the low expansion velocities in K4-37 suggest that the shell might have been decelerated in the course of the evolution.

If this was the case, the 'true' kinematical age of K4-37 would be $<665\times$D[kpc] yr, and 14 kpc could be a lower limit to the distance to make compatible the kinematical age of K4-37 with its evolved nature. In any case, it seems to be clear that K4-37 should be located at a relatively large distance.

3.3 Mass ejection history in K4-37

Our data analysis has shown that K4-37 should be classified as a multi-axis PNe. In addition, a very large elliptical structure has been found at 22 μm surrounding the optical nebula, which probably corresponds to mass ejected in the AGB phase of the progenitor of K4-37. These findings provide information about the formation history of K4-37

According to the properties described in the previous sections, the 22 μm ring probably is a detached shell related to mass ejected during the AGB phase. The emission detected inside the ring indicates that it is filled with material while the bright edge traces the site of interaction between the AGB ejections and the interstellar medium (ISM; e.g. Villaver, García-Segura & Manchado 2002; Schöier, Lindqvist & Olofsson 2005; Mattsson, Höfner & Herwing 2007). Detached shells are observed in many AGB and post-AGB stars (e.g. Speck, Meixner & Knapp 2000; Cox et al. 2012; and references therein). To the best of our knowledge, the 22 μm ring in K4-37 is the largest one of this kind of shells, only comparable to that around R CrB (size ∼8.7 pc, Gillett et al. 1986), and much larger than those around AGB stars (sizes ∼0.04–0.8 pc, e.g. Olofsson et al. 2000; Cox et al. 2012), and post-AGB stars as, e.g. AFGL 2688 and CRL 618 with sizes of ∼4 and ∼6.6 pc, respectively (Speck et al. 2000). Although the evolution of these shells may be complex (e.g. Villaver et al. 2002), detached shells around AGB and post-AGB stars could be expected to grow noticeably when the (possible) associated future PNe reach a highly evolved phase.

The elliptical morphology of the 22 μm ring contradicts the spherical mass ejection that is expected to dominate during the AGB phase (e.g. Olofsson et al. 2000; Kerschbaum et al. 2010). It is interesting to speculate about the origin of this morphology. Deformation of an original spherical AGB shell by the own interaction with the ISM can be ruled out because of the very peculiar ISM structure required to create a well-defined elliptical ring. The 22 μm ring has some resemblance with the 'eye-type' shells observed around some AGB stars (Cox et al. 2012). 'Eye-type' shells have been modelled as deformation of an AGB spherical shell by the ISM magnetic field (van Marle, Cox & Decin 2014) and a similar model could be applicable to the 22 μm ring. Alternatively, a companion could flatten the (spherical) envelope of an AGB star (Mauron, Huggins & Cheung 2013) resulting in an oblated ellipsoidal shell. Molecular line observations of the 22 μm ring are required to study its kinematics, and to derive its 3D structure and properties.

The formation of K4-37 itself fits well into the usual scenario in which several bipolar outflows have shaped the nebula (Sahai & Trauger 1998). As observed in many PNe, the bipolar outflows should have been ejected at different directions and their collimation degree has also changed; a poor collimated outflow seems to be involved in the formation of the bipolar lobes, while more focused outflows could be related to the distortions of the lobes and point-symmetric regions. Our data do not allow us to establish a possible time sequence in the generation of the various outflows, although the bipolar lobes may be ascribed to a major ejection event.

Table 3. Chemical abundances [12+log[n(X)/n(H)] in K4-37 and NGC 6309.

PN	He	N	O	S	Ar	N/O	Reference
K4-37	11.161	8.80	8.43	7.10	6.55	2.32	This work
NGC 6309	11.061	7.94	8.73	6.79	6.47	0.15	Vázquez et al. 2008

3.4 Comparison of K4-37 and NGC 6309

Among multi-axis PNe, we found striking morphological similarities between K4-37 and NGC 6309, a PN with a bright equatorial torus and two pairs of bipolar lobes at different directions (Vázquez et al. 2008; Rubio et al. 2015). Knotty and point-symmetric structures can be recognized in the lobes as well as distortions in one of the pairs of NGC 6309, characteristics that are present in K4-37 as well. Interestingly, the two pairs of bipolar lobes and the torus of NGC 6309 seem to be tilted with respect to the observer by the same amount (Vázquez et al. 2008; Rubio et al. 2015). This implies that if NGC 6309 was observed from a line of sight perpendicular to the current one, it would appear as a 'simple' bipolar PN, with a pair of bipolar lobes and an equatorial torus sharing a single main axis, and resembling the images of K4-37; in this case, only a morphokinematical analysis of NGC 6309 would be able to reveal the existence of two pairs of lobes and different orientations of the structures. Moreover, a spherical halo surrounds NGC 6309 and evidence exists for a large shell with a size of ∼1.5 pc and kinematical age of $\sim1.5\times10^5$ yr (Rubio et al. 2015). This comparison strongly suggests that the central stars of K4-37 and NGC 6309 share a similar mass ejection history. In particular, the specific processes involved in the shaping of the multi-axis structure should have been very similar in both PNe.

Some differences can be noticed between K4-37 and NGC 6309. In particular, the electron density in NGC 6309 (1400–4000 cm^{-3}; Vázquez et al. 2008) does not indicate a particularly young or a highly evolved PN, in consonance with its kinematical age of ∼4000 yr (Vázquez et al. 2008; Rubio et al. 2015) that suggests a moderately young/evolved PN. Probably K4-37 and NGC 6309 are in a different evolutionary stage within PN evolution, being K4-37 in a more advanced one.

However, the most interesting difference between K4-37 and NGC 6309 is observed in their chemical abundances that are listed in Table 3. Although He seems to be slightly overabundant in NGC 6309, N may be deficient, and the N/O abundance ratio is very low. Albeit multi-axis, NGC 6309 is not a type I PN (Vázquez et al. 2008). Chemical abundances in PNe are primarily related to the initial mass of the progenitor. Therefore, K4-37 and NGC 6309 should have evolved from progenitors of very different mass. The chemical abundances in NGC 6309 (Table 3) and the models by Karakas (2010) suggest an initial mass of ∼1–1.2 $M_\odot$ for its progenitor, while 4–6 $M_\odot$ were estimated in the case of K4-37 (see above). Vázquez et al. (2008) noticed that the existence of the multi-axis structure of NGC 6309 strongly contrasts with the idea that these kind of PNe should be associated with intermediate-mass progenitors (e.g. Corradi & Schwarz 1995). The striking structural similarities between K4-37 and NGC 6309 strengthen this conclusion: stars with very different initial mass have been able to shape very similar PNe at the end of their lives. The complexity of K4-37 and NGC 6309 is compatible with that expected from binary central stars and, in particular, from those having evolved through a common envelope phase. It is known that post-common envelope binary central stars tend to be associated with complex PNe that often show multiple structures and/or signs of collimated/focused

outflows (Miszalski et al. 2009; Aller et al. 2015). In NGC 6309, evidence (but not conclusive yet) exists for a possible F3V companion, as suggested by the near-IR excess observed towards its central star (Douchin et al. 2015). In K4-37, such an evidence does not exist. Nevertheless, given the complexity of the nebula, it is reasonable to propose a binary nature for the central star of K4-37.

4 CONCLUSIONS

We have presented and analysed narrow- and broad-band images, intermediate- and high-resolution spectra, and *WISE* archive images of K4-37, a PN not analysed before. The main conclusions of this work can be summarized as follows.

(i) K4-37 appears as a bipolar PN consisting of a bright equatorial torus, two main bipolar lobes, point-symmetric structures and off-axis deformations of the bipolar lobes. Its internal kinematics cannot be reproduced assuming a homologous expansion velocity law. The morphokinematical analysis allows us to disclose the existence of three distinct axes and additional particular directions in K 3-37 that may be classified as a multi-axis PN.

(ii) Very strong [N II], [S II] and relatively strong He II emission lines are observed in the nebular spectrum. High He and N abundances, and a very high N/O abundance ratio ($\sim$2.32) are obtained. A progenitor of $\sim$4–6 $M_{\odot}$ is estimated. The nebula presents a very low electron density indicating a highly evolved PN.

(iii) A distance of $\sim$14 kpc is estimated for K4-37, which is compatible with its highly evolved PN nature and a kinematical age of $\sim 10^4$ yr.

(iv) The *WISE* image at 22 μm reveals K4-37 to be surrounded by a very large elliptical detached shell with a size of $\sim 13 \times 8$ pc^2 and a kinematical age of $\sim 4.3 \times 10^5$ yr. This shell is probably related to the mass ejected during the AGB phase of the progenitor of K4-37.

(v) The elliptical morphology of the detached shell is not compatible with the spherical mass ejection expected in the AGB phase. Deformation of an originally spherical shell by the ISM magnetic field and/or the influence of a companion could explain the peculiar morphology. The formation of the nebula itself is better understood as caused by several focused outflows at different directions and with different collimation degrees.

(vi) Remarkable morphological similarities exist between K4-37 and NGC 6309. However, chemical abundances largely differ in both PNe, indicating progenitors of very different initial mass. These results suggest that the initial mass of the progenitor has not played a crucial role in shaping these two PNe, but their formation can be better attributed to a similar mass-loss history of their central stars that, given the complexity of both PNe, are probably binary.

ACKNOWLEDGEMENTS

We are very grateful to our referee for his/her comments that have helped to improve our analysis, interpretation and presentation of the results. We thank Calar Alto Observatory for allocation of director's discretionary time to this programme. We are very grateful to the staff of Calar Alto for carrying out these observations. We thank the staff of OAN-SPM for assistance during observations. We thank Wolfgang Steffen for interesting discussions and help with SHAPE. This publication makes use of data products from the *Wide-field Infrared Survey Explorer*, which is a joint project of the University of California, Los Angeles and the Jet Propulsion Laboratory/California Institute of Technology, funded by the National Aeronautics and Space Administration. This research is based on observations collected at the German-Spanish Astronomical Center, Calar Alto, jointly operated by the Max-Planck-Institut für Astronomie (Heidelberg) and the Instituto de Astrofísica de Andalucía (CSIC), and upon observations carried out at the Observatorio Astronómico Nacional in the Sierra San Pedro Mártir (OAN-SPM), Baja California, Mexico. LFM acknowledges partial support from Spanish MINECO grant AYA2014-57369-C3-3-P (co-funded by FEDER funds). This project is supported by UNAM-DGAPA-PAPIIT grant IN107914. Part of this paper was done during a stay of LFM at the IA-UNAM (Ensenada, México). He is very grateful to the people of the IA-UNAM for their warm hospitality and pleasant stay.

REFERENCES

Acker A., Marcout J., Ochsenbein F., Stenholm B., Tylenda R.. Schohn C., 1992, The Strasbourg-ESO Catalogue of Galactic Planetary Nebulae, Parts I, II. ESO, Garching
Akras S., Gonçalves D. R., 2016, MNRAS, 455, 930
Akras S., Clyne N., Boumis P., Monteiro H., Gonçalves D. R., Redman M. P., Williams S., 2016, MNRAS, 457, 3409 (AK16)
Aller A., Miranda L. F., Olguín L., Vázquez R., Guillén P. F., Oreiro R., Ulla A., Solano E., 2015, MNRAS, 446, 317
Balick B., 1987, AJ, 94, 671
Balick B., Frank A., 2002, ARA&A, 40, 439
Bermúdez L. C., 2015, MSc thesis, Universidad Nacional Autónoma de México
Blöcker T., 1995, A&A, 299, 755
Chiotellis A., Boumis P., Nanouris N., Meaburn J., Dimitriadis G., 2016, MNRAS, 457, 9
Corradi R. M. L., Schwarz H. E., 1995, A&A, 293, 871
Cox N. L. J. et al., 2012, A&A, 537, A35
de Marco O., 2009, PASP, 121, 316
Dennis T. J., Cunningham A. J., Frank A., Balick B., Blackman E. G., Mitran S, 2008, ApJ, 679, 1327
Douchin D. et al., 2015, MNRAS, 448, 3132
Frew D. J., Parker Q. A., Bojičić I. S., 2016, MNRAS, 455, 1459
García-Segura G., Langer N., Różyczka M., Franco J., 1999, ApJ, 517, 767
Gillett F. C., Backman D. E., Beichman C, Neugebauer G., 1986, ApJ, 310, 842
Jones D., 2016, J. Phys.: Conf. Ser., 728, A032014
Karakas A. I., 2010, MNRAS, 403, 1413
Kerschbaum F. et al., 2010, A&A, 518, L140
Kingsburgh R. L., Barlow M. J., 1994, MNRAS, 271, 257
Kohoutek L., 1965, Bull. Astron. Inst. Czech., 16, 221
Kwok S., Purton C. R., Fitzgerald P. M., 1978, pJ, 219, L125
Mattsson L., Höfner S., Herwing F., 2007, A&A, 470, 339
Mauron N., Huggins P. J., Cheung C.-L., 2013, A&A, 551, A110
Meaburn J., López J. A., Gutiérrez L., Quirós F., Murillo J. M., Valdés J., Pedráyes M., 2003, Rev. Mex. Astron. Astrofis., 39, 185
Miranda L. F., Vázquez R., Torrelles J. M., Eiroa C., López J. A., 1997, MNRAS, 288, 777
Miranda L. F., Vázquez R., Corradi R. L. M., Guerrero M. A., López J. A., Torrelles J. M., 1999, ApJ, 520, 714
Miranda L. F., Fernández M., Alcalá J. M. Guerrero M. A., Anglada G., Gómez Y., Torrelles J. M., Aaquist O. B., 2000, MNRAS, 311, 748
Miranda L. F., Torrelles J. M., Guerrero M. A., Vázquez R., Gómez Y., 2001, MNRAS, 321, 487
Miszalski B., 2012, in Manchado A., Stanghellini L., Schönberner D., eds, Proc. IAU Symp. 283, Planetary Nebulae: An Eye to the Future. Cambridge Univ.Press, Cambridge, p. 107
Miszalski B., Acker A., Parker Q. A., Moffat A. F. J., 2009, A&A, 505, 249
Morris M., 1981, ApJ, 249, 572
Olguín L., Vázquez R., Contreras M. E., Jiménez M. Y., 2011, Rev. Mex. Astron. Astrofis. Ser. Conf., 40, 193

Olofsson H., Bergman P., Lucas R., Eriksson K., Gustafsson B., Bieging J. H., 2000, A&A, 353, 583
Parker Q. A., Bojičić I. S., Frew D. J., 2016, J. Phys.: Conf. Ser., 728, A032008
Peimbert M., 1990, Rep. Prog. Phys., 53, 1559
Pottasch S. R., Beintema D. A., Feibelman W. A., 2000, A&A, 363, 767
Rubio G., Vázquez R., Ramos-Larios G., Guerrero M. A., Olguín L., Guillén P. F., Mata H., 2015, MNRAS, 446, 1931
Sahai R., Trauger J. T., 1998, AJ, 116, 1357
Schöier F. L., Lindqvist M., Olofsson H., 2005, A&A, 436, 633
Seaton M. J., 1979, MNRAS, 187, 73
Soker N., 1994, MNRAS, 270, 774
Soker N., Livio M., 1994, ApJ, 421, 219
Soker N., Rappaport S., Harpaz A., 1998, ApJ, 496, 842
Speck A. K., Meixner M., Knapp G. R., 2000, ApJ, 545, L145
Steffen W., García-Segura G., Koning N., 2009, ApJ, 691, 696
Steffen W., Koning N., Wenger S., Morisset C., Magnor M., 2011, IEEE Trans. Vis. Comput. Graphics, 17, 454
Steffen W., Koning N., Esquivel A, García-Segura G., García-Díaz M. T., López J. A., Magnor M., 2013, MNRAS, 436, 470
Tweedy R. W., Napiwotzki R., 1994, AJ, 108, 948
van Marle A. J., Cox N. L. J., Decin L., 2014, A&A, 570, A131
Vázquez R., Miranda L. F., Torrelles J. M., Olguín L., Benítez G., Rodríguez L. F., López J. A., 2002, ApJ, 576, 860
Vázquez R., Miranda L. F., Olguín L., Ayala S., Torrelles J. M., Contreras M. E., Guillén P. F., 2008, A&A, 481, 107
Villaver E., García-Segura G., Manchado A., 2002, ApJ, 571, 880
Wright E. L. et al., 2010, AJ, 140, 1868

This paper has been typeset from a TEX/LATEX file prepared by the author.